dermal growth factor receptor tyrosine kinase inhibitor, in patients with five selected solid tumor types. J Clin Oncol 2002;20:4292–302.
[2] Fukuoka M, Yano S, Giaccone G, Tamura T, Nakagawa K, Douillard JY, et al. Multi-institutional randomized phase II trial of gefitinib for previously treated patients with advanced non-small-cell lung cancer. J Clin Oncol 2003;21:2237–46.
[3] Giaccone G, Herbst RS, Manegold C, Scagliotti G, Rosell R, Miller V, et al. Gefitinib in combination with gemcitabine and cisplatin in advanced non-small-cell lung cancer: a phase III trial—INTACT 1. J Clin Oncol 2004;22:777–84.
[4] Kris MG, Natale RB, Herbst RS, Lynch Jr TJ, Prager D, Belani CP, et al. Efficacy of gefitinib, an inhibitor of the epidermal growth factor receptor tyrosine kinase, in symptomatic patients with non-small cell lung cancer: a randomized trial. JAMA 2003;290:2149–58.
[5] Rusch V, Baselga J, Cordon-Cardo C, Orazem J, Zaman M, Hoda S, et al. Differential expression of the epidermal growth factor receptor and its ligands in primary non-small cell lung cancers and adjacent benign lung. Cancer Res 1993;53:2379–85.
[6] Lynch TJ, Bell DW, Sordella R, Gurubhagavatula S, Okimoto RA, Brannigan BW, et al. Activating mutations in the epidermal growth factor receptor underlying responsiveness of non-small-cell lung cancer to gefitinib. New Eng J Med 2004;350:2129–39.
[7] Paez JG, Jänne PA, Lee JC, Tracy S, Greulich H, Gabriel S, et al. *EGFR* mutations in lung cancer: correlation with clinical response to gefitinib therapy. Science 2004;304:1497–500.
[8] Pao W, Miller V, Zakowski M, Doherty J, Politi K, Sarkaria I, et al. EGF receptor gene mutation are common in lung cancer from "never smokers" and are associated with sensitivity of tumors to gefitinib and elrotinib. Proc Natl Acad Sci USA 2004;101:13306–11.
[9] Sordella R, Bell DW, Haber DA, Settleman J. Gefitinib-sensitizing *EGFR* mutations in lung cancer activate anti-apoptotic pathways. Science 2004;305:1163–7.
[10] Tracy S, Mukohara T, Hansen M, Meyerson M, Johnson BE, Jänne PA. Gefitinib induces apoptosis in the *EGFR* L858R non-small cell lung cancer cell line H3255. Cancer Res 2004;64:7241–4.
[11] Hampe J, Wollstein A, Lu T, Frevel HJ, Will M, Manaster C, et al. An integrated system for high throughput TaqMan based SNP genotyping. Bioinformatics 2001;17:654–5.
[12] Mc Guigan FE, Ralston SH. Single nucleotide polymorphism detection: allelic discrimination using TaqMan. Psychiatr Genet 2002;12:133–6.
[13] Ranade K, Chang MS, Ting CT, Pei D, Hsiao CF, Olivier M, et al. High-throughput genotyping with single nucleotide polymorphisms. Genome Res 2001;11:1262–8.
[14] Shi MM, Bleavins MR, de la iglesia FA. Technologies for detecting genetic polymorphisms in pharmacogenomics. Mol Diagn 1999;4:343–51.
[15] Shi MM. Enabling large-scale pharmacogenetic studies by high-throughput mutation detection and genotyping technologies. Clin Chem 2001;47:164–72.
[16] Tanaka C, Kamide K, Takiuchi S, Miwa Y, Yoshii M, Kawano Y, et al. An alternative fast and convenient genotyping method for the screening of angiotensin converting enzyme gene polymorphisms. Hypertens Res 2003;26:301–6.
[17] Robledo R, Beggs W, Bender P. A simple and cost-effective method for rapid genotyping of insertion/deletion polymorphisms. Genomics 2003;82:580–2.
[18] Sasaki H, Endo K, Konishi A, Takada M, Kawahara M, Iuchi K, et al. *EGFR* mutation status in Japanese lung cancer patients: genotyping analysis using LightCycler. Clin Cancer Res 2005;11:2924–9.
[19] Jänne PA, Gurubhagavatula S, Yeap BY, Lucca J, Ostler P, Skarin AT, et al. Outcomes of patients with advanced non-small cell lung cancer treated with gefitinib (ZD1839, "Iressa") on an expanded access study. Lung Cancer 2004;44:221–30.
[20] Hirsch FR, Varella-Garcia M, Bunn Jr PA, Di Maria MV, Veve R, Bremmes RM, et al. Epidermal growth factor receptor in non-small-cell lung carcinomas: correlation between gene copy number and protein expression and impact on prognosis. J Clin Oncol 2003;21:3798–807.
[21] Cappuzzo F, Hirsch FR, Rossi E, Bartolini S, Ceresoli GL, Bemis L, et al. Epidermal growth factor receptor gene and protein and gefitinib sensitivity in non-small-cell lung cancer. J Natl Cancer Inst 2005;97:643–55.
[22] Chen YC, Chen JH, Richard K, Chen PY, Christiani DC. Lung adenocarcinoma and human papillomavirus infection. Cancer 2004;15:1428–36.
[23] Kosaka T, Yatabe Y, Endoh H, Kuwano H, Takahashi T, Mitsudomi T. Mutations of the epidermal growth factor receptor gene in lung cancer: biological and clinical implications. Cancer Res 2004;64:8919–23.
[24] Huang S-F, Liu HP, Li LH, Ku YC, Fu YN, Tsai HY, et al. High frequency of epidermal growth factor receptor mutations with complex patterns in non-small cell lung cancers related to gefitinib responsiveness in Taiwan. Clin Cancer Res 2004;10:8195–203.
[25] Arao T, Fukumoto H, Takeda M, Tamura T, Saijo N, Nishio K. Small in-frame deletion in the epidermal growth factor receptor as a target for ZD6474. Cancer Res 2004;64:9101–4.

DOI 10.1002/pmic.200401145 *Proteomics* 2005, *5*, 1150–1159

REGULAR ARTICLE

# Clinical-scale high-throughput human plasma proteome analysis: Lung adenocarcinoma

*Kiyonaga Fujii*[1], *Tomoyo Nakano*[1], *Mitsuhiro Kanazawa*[3], *Shingo Akimoto*[3], *Takashi Hirano*[2], *Harubumi Kato*[2] *and Toshihide Nishimura*[1,3]

[1] Clinical Proteome Center
[2] Department of Surgery, Tokyo Medical University, Shinjuku, Tokyo, Japan
[3] Medical ProteoScope Co., Ltd., Shinjuku, Tokyo, Japan

Received: May 14, 2004
Revised: October 13, 2004
Accepted: November 15, 2004

Clinical proteomics requires the stable and reproducible analysis of a large number of human samples. We report a high-throughput comprehensive protein profiling system comprising a fully automated, on-line, two-dimensional microflow liquid chromatography/tandem mass spectrometry (2-D μLC-MS/MS) system for use in clinical proteomics. A linear ion-trap mass spectrometer (ITMS) also known as a 2-D ITMS instrument, which is characterized by high scan speed, was incorporated into the μLC-MS/MS system in order to obtain highly improved sensitivity and resolution in MS/MS acquisition. This system was used to evaluate bovine serum albumin and human 26S proteasome. Application of these high-throughput μLC conditions and the 2-D ITMS resulted in a 10-fold increase in sensitivity in protein identification. Additionally, peptide fragments from the 26S proteasome were identified three-fold more efficiently than by the conventional 3-D ITMS instrument. In this study, the 2-D μLC-MS/MS system that uses linear 2-D ITMS has been applied for the plasma proteome analysis of a few samples from healthy individuals and lung adenocarcinoma patients. Using the 2-D and 1-D μLC-MS/MS analyses, approximately 250 and 100 different proteins were detected, respectively, in each HSA- and IgG-depleted sample, which corresponds to only 0.4 μL of blood plasma. Automatic operation enabled the completion of a single run of the entire 1-D and 2-D μLC-MS/MS analyses within 11 h. Investigation of the data extracted from the protein identification datasets of both healthy and adenocarcinoma groups revealed that several of the group-specific proteins could be candidate protein disease markers expressed in the human blood plasma. Consequently, it was demonstrated that this high-throughput μLC-MS/MS protein profiling system would be practically applicable to the discovery of protein disease markers, which is the primary objective in clinical plasma proteome projects.

**Keywords:**
Clinical Proteomics / Human plasma / Linear ion-trap mass spectrometry / Lung adenocarcinoma / Plasma proteome

**Correspondence:** Professor Toshihide Nishimura, Professor of Clinical Proteome Center, Tokyo Medical University, 2-6-1, Nishi-shinjuku, Shinjuku-ku, Tokyo 163-0217, Japan
**E-mail:** nisimura@tokyo-med.ac.jp
**Fax:** +1-81-3-5321-6624

**Abbreviations: ABC**, ammonium bicarbonate; **AID-HP**, albumin-and-IgG-depleted human plasma; **IAM**, iodoacetamide; **Ig**, immunoglobulin; **ITMS**, ion-trap mass spectrometry; **μLC**, microflow liquid chromatography; **NSI**, nanoelectrospray ionization; **SCX**, strong cation exchange; **TCEP**, tris[2-carboxyethyl]phosphine; **TPX**, methylpentene polymer

## 1 Introduction

Human blood plasma is generally the most informative proteome from a medical viewpoint, because it is the primary clinical specimen and it also represents the largest and deepest version of human proteome present in any sample [1–3]. Almost all body cells communicate with the plasma either directly or through tissues/biological fluids, and many of these cells release at least a part of their contents into the plasma upon damage or death. A comprehensive, systematic characterization of the plasma proteome in the healthy and

diseased states will greatly facilitate the development of biomarkers for early disease detection, clinical diagnosis, and therapy of cancer and other diseases. However, broad characterization of the human plasma proteome may pose one of the greatest challenges. This is because it can contain low-level proteins, which are secreted by solid tissues, as well as other important proteins (tissue leakage proteins at pg/mL levels) in the presence of several relatively dominant, high-abundance proteins (particularly HSA at 35–50 mg/mL). The dynamic range of plasma protein concentrations minimally spans nine orders of magnitude. For clinical and diagnostic proteomics using human plasma, it is essential to develop a comprehensive system, which has a high resolution and a wide dynamic range, for large-scale proteome analysis.

Recently, multi-dimensional LC-MS/MS has been developed as a powerful tool, particularly for comprehensive identification of highly complex proteins. This method can achieve a resolving power that is equal to or higher than 2-DE [4–6]. Broad protein identification techniques can detect specific proteins present in low concentrations in a highly complex protein matrix. To characterize the human plasma proteome, Smith *et al.* have achieved a protein identification dynamic range of more than eight orders of magnitude using 2-D LC combined with conventional ion-trap MS/MS instrumentation [6]. This approach has resulted in the identification of >800 plasma proteins from 5 μL plasma without the depletion of highly abundant HSA and/or immunoglobulins (Ig). The multi-dimensional LC-MS/MS techniques reported thus far indicate the potential usefulness of broad protein identification with high resolution and wide dynamic range for cataloging the plasma contents. However, these approaches require further improvement in terms of both ease of use and industrial applicability to routine clinical use, because their application to clinical research requires stable and reproducible analyses of a large number of human samples.

The establishment of a simple, robust, and high-throughput protein profiling system as a global platform is extremely important from the viewpoint of clinical proteomics. This is because a large number of human tissue/biological fluid samples could then be quantitatively analyzed, in a routine and reproducible manner, for expressed proteins. Such a system would help discover any protein that is significantly associated with a specific disease status. We have constructed a technically well integrated and high-throughput LC-MS/MS system with RP microflow LC (μLC) and a conventional ion-trap MS/MS equipped with a nanoelectrospray ionization (NSI) interface to detect lung cancer biomarkers and to analyze apoptotic mechanisms [7, 8]. Additionally, the system has been combined with on- or off-line strong cation-exchange (SCX) chromatography to result in a multi-dimensional protein profiling system. This protein profiling system using off-line 2-D SCX/RP μLC-MS/MS was successfully applied to broad protein identification of human plasma proteins [9]. We have also established protein depletion, in-solution digestion, and data-integrating/mining systems with an automated operation for large-scale human plasma proteome analysis.

The dynamic range and sequence coverage that results from protein identification by LC-MS/MS analysis depends on both the quality of the separation(s) applied and the MS platform [6]. When resolution performance is not considered, the quality of the 2-D LC is substantially related to the number of fractionation steps for the first dimension chromatography and the analytical running time for the second dimension chromatography. Since the dynamic range of the MS platform is based on the performance of the instrument used, the number of the MS/MS acquisition in one run strictly depends on both the scan speed and the analytical time required by the LC-MS/MS analysis. Recently, linear ion-trap MS/MS (2-D ITMS) instruments with a higher scan speed and sensitivity than conventional 3-D ITMS instruments have emerged as new generation instruments. Therefore, we applied the new 2-D ITMS instrument to the fully automated on-line 2-D μLC-MS/MS system developed by us [10].

In this study, we evaluated the performance of the μLC-MS/MS system using the 2-D ITMS instrument for extending the sensitivity, dynamic range, and coverage for comprehensive protein identification. BSA and human 26S proteasome were used as the authentic protein sample and the protein complex sample, respectively. The system, together with the on-line 2-D μLC-MS/MS system, was then applied to proteome analysis of human plasma; HSA- and IgG-depleted samples were obtained from a few healthy individuals and lung adenocarcinoma cases.

## 2 Materials and methods

### 2.1 Materials

HPLC-grade ACN, formic acid, and TFA were purchased from Wako Pure Chemical Industries, Ltd. (Osaka, Japan). Milli-Q grade water (Millipore, Bedford, MA, USA) was used. BSA, ammonium formate, ammonium bicarbonate (ABC), and iodoacetamide (IAM) were purchased from Sigma (St. Louis, MO, USA). Human 26S proteasome (PW9310) was obtained from Affiniti Research Products (Devon, UK). Tris[2-carboxyethyl]phosphine (TCEP) was purchased from Pierce (Rockford, IL, USA). Sequencing grade-modified trypsin was purchased from Promega (Madison, WI, USA).

### 2.2 Preparation of the digested BSA and human 26S proteasome samples

BSA (1 nmol) was diluted with 225 μL ABC (aq., 100 mM); then, 12.5 μL TCEP (10 mM) was added for reduction and the solution mixture was kept at 37°C for 45 min. Further, 12.5 μL IAM (50 mM) was added, and the solution mixture was alkylated in the dark at 24°C for 1 h. The resulting solution was digested with trypsin (trypsin:protein = 1:50, w/w),

and the resultant 250 μL solution was incubated in the dark at 37°C for 15 h. In-solution digestion of the 26S proteasome sample was carried out as follows: 26S proteasome sample (50 μg) was diluted with ABC (aq., 50 mM) containing 10% v/v ACN to a final volume of approximately 190 μL. For reduction, 2.5 μL TCEP (10 mM) was added, and the solution mixture was kept at 37°C for 45 min. Subsequently, 2.5 μL IAM (50 mM) was added, and the solution mixture was alkylated in the dark at 24°C for 1 h. For digestion, trypsin (2 μg) was added to 5 μL ABC (50 mM), and 200 μL of the resulting solution was incubated in the dark at 37°C for 18 h. All reactions were performed in methylpentene polymer (TPX) microtubes (Hitech Inc. Tokyo, Japan) using an Eppendorf thermomixer R (Brinkmann, Westbury, NY, USA) for 1.5 mL microtubes; the resulting solution was interval-mixed (10 s) at 850 rpm. The digested 26S proteasome sample (50 μL) was diluted with 125 μL of 2% v/v ACN (aq.) containing 0.005% v/v TFA (aq.) after adjusting the pH to approximately 3 with 50 μL of 1% v/v TFA (aq.); the samples (25 μL) were then injected into the μLC-MS/MS system described in this paper.

### 2.3 Sample preparation of the digested human plasma protein mixture

The human blood plasma samples treated with heparin were obtained from Tokyo Medical University (Tokyo, Japan) and acquired from three, healthy, anonymous, male donors (samples: H-N, H-I, and H-S) and two male donors who were diagnosed with adenocarcinoma on the basis of clinical and laboratory criteria (stage: IIIA, samples: AC88 and AC94), after obtaining their informed consent. HSA and IgG in the human plasma samples (500 μL) was removed by affinity adsorption chromatography using Bio-Rad's Affi-Gel Blue Gel and protein A column (Bio-Rad Hercules, CA, USA), respectively (details not shown). The final concentration of the resulting HSA- and IgG-depleted human plasma (AID-HP) samples were 4.1 (H-N), 8.6 (H-I), 6.6 (H-S), 5.8 (AC88), and 7.2 mg/mL (AC94) in ABC (25 mM). Subsequently, 100 μL of the AID-HP sample was diluted with 400 μL ABC (25 mM) containing 32% v/v ACN. For reduction, 25 μL TCEP (50 mM) was added and the solution mixture was kept at 37°C for 45 min. Subsequently, 25 μL IAM (250 mM) was added and the solution mixture was alkylated in the dark at 24°C for 1 h. For digestion, trypsin (5 μg) was added and the resulting solution (555 μL) was incubated in the dark at 37°C for 16 h. All these reactions were carried out using the Eppendorf thermomixer R for 1.5 mL TPX microtubes, and the mixing was carried out at 850 rpm with periods and intervals of 10 s each. For the 1-D μLC-MS/MS analysis, the digested AID-HP samples (20 μL) were diluted with 20 μL of 1% v/v TFA (aq.) and 160 μL with 2% v/v ACN (aq.) containing 0.1% v/v TFA, in a TPX auto sampler tube; 20 μL of the resultant samples was injected into the system. In order to prepare individual mixture samples of the healthy and adenocarcinoma groups for 1-D and 2-D μLC-MS/MS analyses, 33.3 μL of each of the three AID-HP samples from the healthy group and 50 μL of each of the two AID-HP samples from the adenocarcinoma group were mixed with 100 μL of 1% v/v TFA (aq.), respectively; subsequently, 4 μL of the resulting sample solutions was used in these analyses.

### 2.4 1-D RP and 2-D SCX/RP μLC-NSI-MS/MS analyses

The 1-D and 2-D LC-MS/MS system with RP-μLC comprised a Paradigm MS4 dual solvent delivery system (Michrom BioResources, Auburn, CA, USA) for HPLC, an HTS PAL auto sampler with two 10-port injector valves (CTC Analytics, Zwingen, Switzerland), Finnigan LCQ Deca XP plus 3-D ion-trap, and Finnigan LTQ linear ITMS (Thermo Electron, San Jose, CA, USA) equipped with NSI sources (AMR Inc., Tokyo, Japan). Sample injection for the 1-D and 2-D μLC-MS/MS analyses as well as SCX separation for 2-D analysis were automatically carried out using the HTS PAL auto sample injection system with no change in the configurations. The SCX separation was performed on an SCX microtrap cartridge (12 μm, 300 Å, 8 × 1.0 mm i.d., Michrom) by stepwise elution on the first injector valve. The solvent system containing 2% v/v ACN was composed of 0.005% v/v TFA (aq.) and 1 M ammonium formate (aq.) adjusted to pH 2.8 with TFA, and the elution solvents (25, 50, 100, 150, 200, and 500 mM) were prepared by mixing these. The effluent from all the SCX fractions was flowed serially into a peptide CapTrap cartridge (2.0 × 0.5 mm i.d., Michrom), present on the second injector valve, for concentration and desalting. After desalting with 0.1% v/v TFA (aq.) containing 2% v/v ACN, the sample was loaded onto a capillary RP column, MAGIC $C_{18}$ (3 μm, 200 Å, 50 × 0.2 mm i.d., Michrom), for 2-D separation. Digested samples for the 1-D RP analysis were also injected directly into a peptide CapTrap cartridge for concentration and desalting and then applied to RP separation. Solutions of 2% and 90% v/v ACN (aq.) were used as the mobile phases A and B, respectively, and both contained 0.1% v/v formic acid. The gradient conditions in the chromatographic run were as follows: B 5% (0 min) → 65% (20 min) for the digested samples of BSA and 26S proteasome, and B 5% (0 min) → 40% (70 min) → 95% (80 min) for plasma samples. Effluent solvent at 1.0–1.2 μL/min from the HPLC was introduced into the mass spectrometer by the NSI interface *via* an injector valve with a CapTrap cartridge and the RP column. The NSI needle (FortisTip, OmniSeparo-TJ, Hyogo, Japan), which was connected directly to the RP column outlet, was used as the NSI interface and the voltage was 1.8 kV, while the capillary was heated to 200°C [11]. No sheath or auxiliary gas was used. Further, the mass spectrometer was operated in a data-dependent acquisition mode in which MS acquisition with a mass range of $m/z$ 450–2000 was automatically switched to MS/MS acquisition under the automated control of the Xcalibur software. The most intense ion of the full MS scan was selected as the parent ion and it was subjected to MS/MS scan with an isolation width of $m/z$ 2.0; the activation amplitude parameter

was set at 30%. For the human plasma samples, the full MS scan was acquired followed by two successive MS/MS scans of the two most intense precursor ions detected in the full MS scan. The trapping time was 100 ms under the auto gain control mode. Data was acquired using the dynamic mass-exclusion windows that had an exclusion of 3.0-min duration and exclusion mass widths of −0.5 and +1.5 Da.

### 2.5 Database searches

All MS/MS data were investigated using the Mascot search engine (Matrix Science, London, UK) [12] against the Swiss-Prot database. The data acquired for BSA digests were investigated against other mammalian subsets of the sequences. The MS/MS data of the human 26S proteasome and plasma samples were investigated against the *Homo sapien* subsets of the sequences. The database searches allowed for fixed modification on the cysteine residue (carbamidomethylation, +57 Da), variable modification on the methionine residue (oxidation, +16 Da), peptide mass tolerance at ±2.0 Da, and fragment mass tolerance at ±0.8 Da.

## 3 Results and discussion

### 3.1 Evaluation of the μLC-MS/MS analysis using the linear 2-D ITMS instrument

We developed the μLC-MS/MS system with RP separation (1-D RP), which corresponds to the second dimension separation for the on-line and off-line 2-D μLC-MS/MS system [9, 10]. This system comprises a microflow LC system with a variable splitter, a versatile auto-sampler equipped with an injector valve, and a LCQ 3-D (ITMS) with an NSI stage. A flow rate of 1.0–1.2 μL/min *via* the injector valve and the RP column (0.2 mm i.d.) has been adopted as a convenient and efficient condition for routine proteome analysis with high sensitivity and reproducibility. The detection limit for identification of proteins in protein digests was approximately a few fmol. In order to evaluate the sensitivity of the new linear 2-D ITMS instrument (LTQ) for protein identification, we connected our RP μLC system to the LTQ instead of the conventional 3-D ITMS (LCQ) instrument. BSA digests (5–500 fmol) were applied to μLC-MS/MS analysis using the LTQ and LCQ instruments under identical conditions except those used for the mass spectrometer. The base-peak chromatogram for BSA digests (500 fmol) is shown in Fig. 1a. A comparison of the coverage, in terms of protein identification, between the LCQ and LTQ instruments revealed that 25% coverage of the BSA sequence was acquired from 5 fmol of the digests using the LTQ instrument, as shown in Fig. 2. Since the same coverage was obtained from 50 fmol of the digests using the LCQ instrument, the results indicated that the protein identification improved markedly as the sensitivity increased 10-fold using the LTQ instrument.

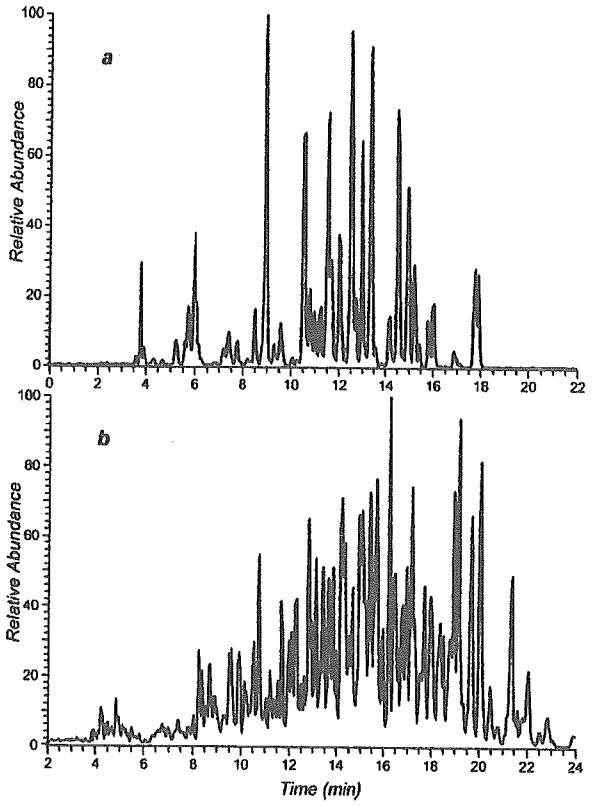


**Figure 1.** Base-peak chromatograms of the digested BSA (a) and 26S proteasome (b) using 1-D RP μLC-MS/MS analysis.

A dramatic improvement is achieved in the LTQ instrument in terms of the scan speed, which is higher than that of conventional 3-D ITMS instruments. Figures 3a and 3b show the expanded mass chromatograms with stick plotting at *m/z* values 710.0–711.5 obtained by μLC-MS/MS analysis of BSA digests using the LTQ and LCQ instruments, respectively. A stick in the peak represents a single full MS or MS/MS scan. The range denoted by the arrow in Fig. 3 shows that 62 events that carried out the acquisition of a full MS and an MS/MS spectra were achieved by the LTQ instrument in comparison with 12 events acquired by the LCQ instrument in 30 s. When conventional LCQ instruments are used, we usually apply three and two microscans for full MS (50 ms trapping time) and MS/MS (200 ms) accumulations, respectively, in order to obtain a better quality spectrum from a single scan. On the other hand, both spectra for peptide sequencing in protein identification were effectively acquired by one microscan of both full MS (50 ms) and MS/MS (100 ms) accumulations by LTQ instrument. As a result, using the LTQ instrument, it is possible to obtain an approximately five-fold higher number of MS/MS spectra in the same analytical run time.

In general, it is necessary to acquire a greater number of MS/MS spectra for the identification of a greater number of proteins using peptide sequencing. In studies where LC-MS/

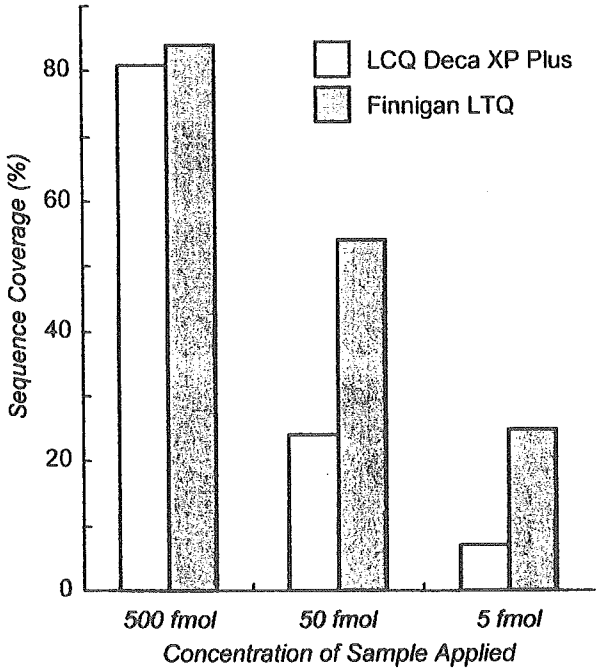


**Figure 2.** Comparison of sequence coverage of BSA digests (5–500 fmol) by μLC-MS/MS analysis using LCQ Deca XP plus 3-D ion-trap and Finnigan LTQ linear ion-trap MS instruments.

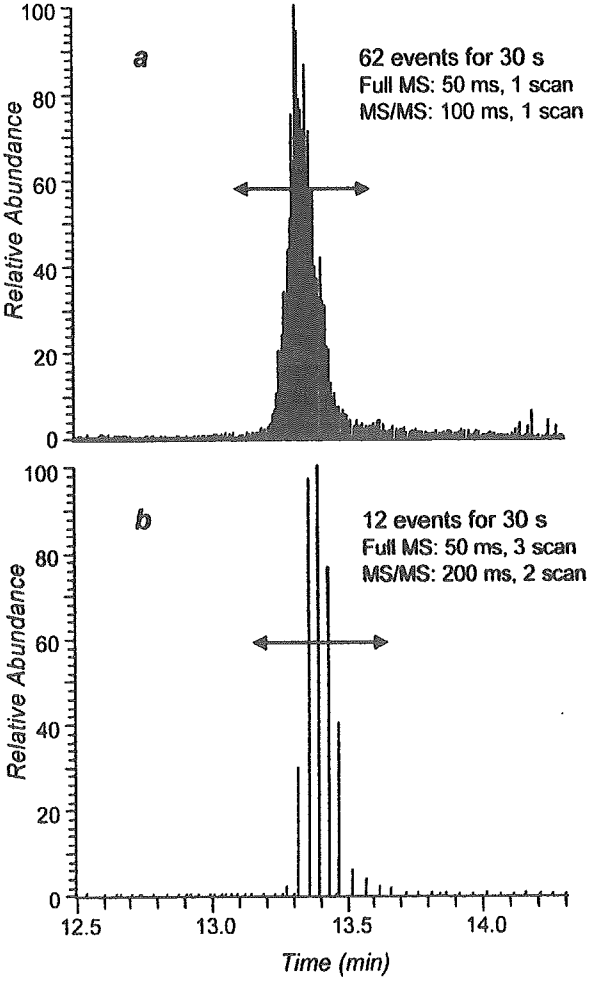


**Figure 3.** Mass chromatograms at *m/z* 710.0-711.5 by μLC-MS/MS analysis of BSA digests using Finnigan LTQ (a) and LCQ Deca XP plus (b) instruments. A stick in the peak is a single full MS and MS/MS scan of the mass spectrometer, and 62 and 12 events (acquisition of a full MS and a MS/MS in one event) were carried out by the LTQ and LCQ instruments, respectively.

MS was used for comprehensive proteome analysis, several researchers investigated various methods to data-dependently amass MS/MS spectra for a single analysis. These methods include employing a longer analytical time, triple and more MS/MS acquisition against a single full MS spectrum, multiple analyses of the same sample using common conditions or fractionated mass range, etc. While obtaining the MS/MS spectra, the scan speed is a mechanical limitation and a data-dependent scan misses many of the peptide sequences for low abundance peaks that are behind large peaks. Therefore, it is necessary to choose the applications of these techniques for comprehensive proteome analysis of highly complex protein mixtures such as human plasma and whole cell lysates. The drawbacks of clinical proteomics for a large number of human samples are the inability to conduct multiple analyses of the same sample and the longer running time required by the comprehensive LC-MS/MS analysis. Consequently, the performance of the LTQ instrument with a higher scan speed is better than that of the conventional 3-D ITMS instrument, because it enables more informative high-throughput LC-MS/MS analysis for highly complex clinical samples. Therefore, to verify the applicability of LTQ instruments, the human 26S proteasome, which is a highly complex protein mixture consisting of 31 components, was subjected to analysis. As shown in Fig. 1b, equivalent amounts of the digested 26S proteasome sample were analyzed using the LCQ and LTQ instruments under identical μLC conditions. The data-dependent MS/MS acquisition, in which the full MS acquisition is followed by a single MS/MS scan of the most intense precursor ion obtained from the full MS scan, was applied with three microscan full MS (50 ms trapping time) and two microscan MS/MS (200 ms) accumulations for the LCQ, and one microscan of both full MS (50 ms) and MS/MS (100 ms) accumulations for the LTQ instruments. During the 20 min analysis, approximately 450 and 2200 MS/MS spectra were obtained from the 1-D RP μLC-MS/MS analyses using the LCQ and LTQ instruments, respectively. These data were evaluated using a Mascot database search against the Swiss-Prot database, and the search results obtained for the peptide MS/MS assignment were filtered based on the criterion defined as a Mascot peptide score more than 20 and ranked first, described in detail below. Table 1 (see also Supplemen-

**Table 1.** Protein identification results of human 26S proteasome.

| Protein | LCQ Deca XP Plus | | | Finnigan LTQ | | |
|---|---|---|---|---|---|---|
| | Score | Coverage | Peptide | Score | Coverage | Peptide |
| 26S protease regulatory subunits | | | | | | |
| PRS4 | 221 | 13 | 3 | 851 | 41 | 16 |
| PRS6 | 142 | 9 | 3 | 757 | 48 | 16 |
| PRS7 | 348 | 15 | 5 | 1346 | 55 | 23 |
| PRS8 | 299 | 16 | 4 | 1304 | 58 | 20 |
| PRSA | 377 | 21 | 7 | 1093 | 53 | 19 |
| PRSX | 154 | 7 | 2 | 715 | 36 | 12 |
| Proteasome subunit alpha types | | | | | | |
| PSA1 | 494 | 36 | 8 | 658 | 48 | 11 |
| PSA2 | 261 | 18 | 4 | 569 | 56 | 9 |
| PSA3 | 145 | 13 | 3 | 584 | 43 | 11 |
| PSA4 | 115 | 9 | 2 | 459 | 33 | 7 |
| PSA5 | 158 | 17 | 3 | 483 | 47 | 8 |
| PSA6 | 559 | 38 | 8 | 700 | 48 | 11 |
| PSA7 | 423 | 35 | 7 | 772 | 57 | 12 |
| Proteasome subunit beta types | | | | | | |
| PSB1 | 275 | 34 | 5 | 596 | 53 | 10 |
| PSB2 | 256 | 24 | 4 | 456 | 43 | 8 |
| PSB3 | 235 | 24 | 3 | 379 | 35 | 5 |
| PSB4 | 117 | 9 | 2 | 511 | 48 | 8 |
| PSB5 | 528 | 42 | 7 | 670 | 58 | 10 |
| PSB6 | 200 | 13 | 3 | 271 | 24 | 5 |
| PSB7 | 232 | 14 | 4 | 381 | 33 | 7 |
| PSB8 | ND | ND | ND | 180 | 18 | 4 |
| 26S proteasome non-ATPase regulatory subunits | | | | | | |
| PSD1 | 227 | 6 | 3 | 1636 | 38 | 27 |
| PSD2 | 380 | 10 | 6 | 1386 | 34 | 26 |
| PSD3 | 690 | 24 | 10 | 1445 | 50 | 25 |
| PSD4 | 74 | 5 | 1 | 358 | 22 | 6 |
| PSD6 | 206 | 12 | 3 | 1001 | 46 | 18 |
| PSD7 | 250 | 15 | 3 | 487 | 42 | 10 |
| PSD8 | ND | ND | ND | 228 | 19 | 5 |
| PSDB | 571 | 22 | 8 | 1445 | 59 | 23 |
| PSDC | 359 | 15 | 5 | 1147 | 37 | 20 |
| PSDD | 183 | 10 | 4 | 966 | 52 | 17 |
| | | Total | 130 | | Total | 409 |

The protein identification data of 31 components consisted of human 26S proteasome including the number of the peptide fragments assigned (Peptide) and the sequence coverage according to these peptides (Coverage). The protein score is calculated by the addition of these peptide scores (Score) in comparison to 1-D μLC-MS/MS analysis using conventional 3-D ion-trap MS (LCQ Deca XP Plus) and new linear ion-trap MS instruments (Finnigan LTQ). ND, not detected.

tary Table A) shows protein identification results including the number of peptide fragments assigned, sequence coverage with these peptides, and the protein score calculated by addition of these peptide scores with respect to the 31 components of the 26S proteasome. In the case of the LTQ instrument, 409 peptide fragments were assigned as components of the 26S proteasome, and this number was approximately three-fold higher than that obtained when the LCQ instrument was used (130 peptide fragments). The individual components of the 26S proteasome were identified by 13.2 and 4.5 peptide fragments, 43.0% and 18.1% sequence coverage, and 821.9 and 292.4 protein scores on an average, using the LTQ and LCQ instruments, respectively. Twenty-nine proteins in 31 components were identified even by the LCQ instruments using our RP μLC system with high-resolution power, as shown in Fig. 1b. However, the peptide fragments of the remaining two components were not observed from the filtered database search results. A number

of peptide fragments belonging to the 26S proteasome (>700 peptides and >60% coverage on an average) were detected by an on-line 2-D SCX/RP μLC-MS/MS experiment with the same amount of digests using the LCQ instrument [10]. These results may simply indicate the difference in the scan speed for the limited, short analytical time between the LCQ and LTQ instruments and not a difference in the sensitivity. Accordingly, LC-MS/MS analysis using LTQ has a three-fold higher efficiency in identification in comparison with a conventional LCQ. This indicates that the LTQ has a superior protein identification capability. Thus, the introduction of LTQ into our μLC-MS/MS system resulted in a highly improved performance, in terms of both sensitivity and protein identification efficiency, for highly complex mixtures.

### 3.2 Human plasma proteome analysis

The usefulness and applicability of our automated protein profiling system coupled with LTQ for clinical proteomics have been examined by analyzing human plasma samples. In the course of clinical plasma proteome studies, we investigated two types of human plasma – one from healthy donors and the other from donors with lung adenocarcinoma. All plasma samples obtained from the three healthy (H-N, H-I, and H-S) and two adenocarcinoma (AC88 and AC94) cases were digested in a solution with trypsin after removing their HSA and IgG contents. The resultant peptide mixtures were diluted for the μLC-MS/MS analysis. Further, equivalent mixture samples from the three healthy donors (H-NIS; H-N:H-I:H-S, 1:1:1 in volume) and the two adenocarcinoma donors (AC8894; AC88:AC94, 1:1 in volume) were also prepared as average samples for each case. The individual and mixture samples (total seven samples) were analyzed by 1-D RP μLC-MS/MS analysis under analytical conditions for 90 min. The LTQ MS data was acquired by the double MS/MS method, in which the full MS acquisition is followed by two MS/MS scans of the two most intense precursor ions from the full MS scan. This is done to improve the protein identification results by the database search. Additionally, our established on-line 2-D SCX/RP μLC-MS/MS system using LTQ instead of the conventional LCQ instrument was also used to analyze the mixture samples (H-NIS and AC8894) along with an additional 1-D RP analysis. In the 2-D μLC-MS/MS analysis, six SCX separation runs were automatically carried out and analyzed by the RP μLC-MS/MS analysis under the same analytical conditions as described earlier. The total operation time for both 1-D and 2-D μLC-MS/MS analyses of a sample was within 11 h [10]. Figure 4 shows the base-peak chromatograms from 1-D (g) and 2-D

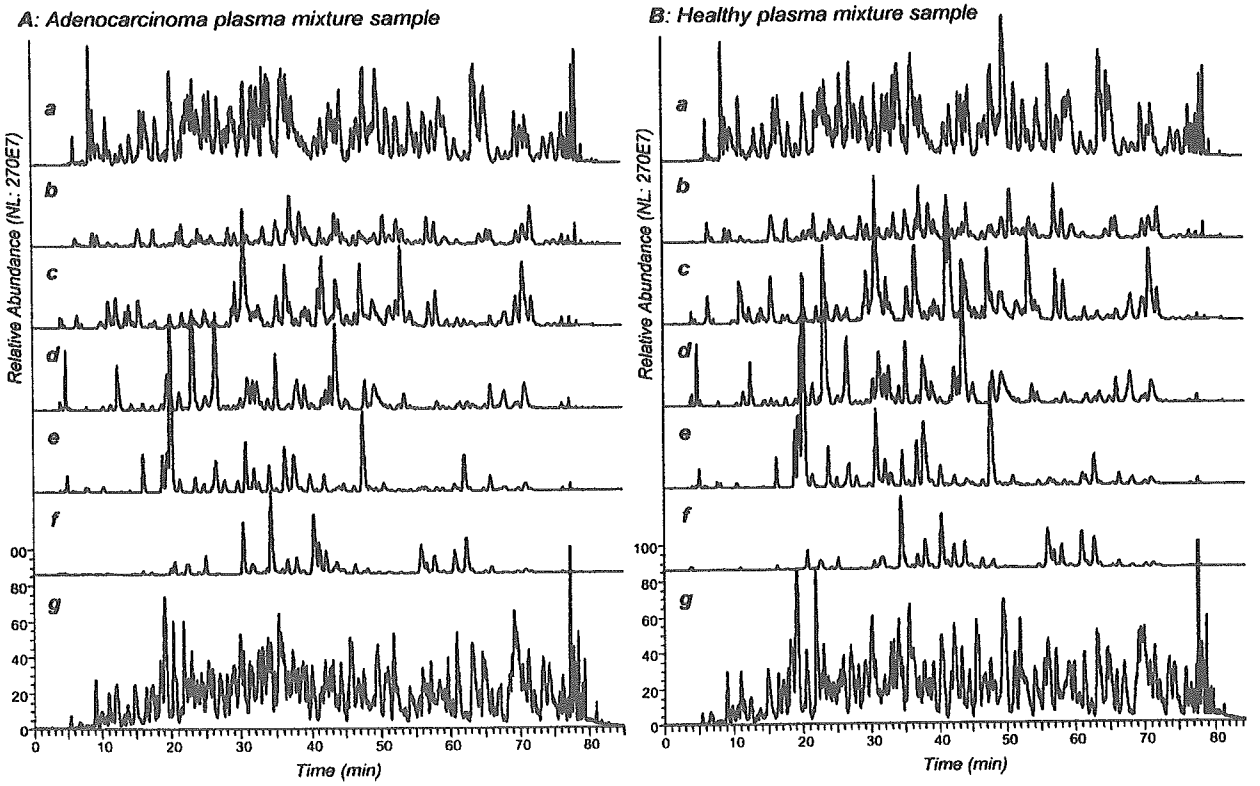


**Figure 4.** Base-peak chromatograms of the digested human plasma samples using 2-D SCX/RP (a–f) and 1-D RP μLC-MS/MS analyses (g). A, mixture of plasma digests of the healthy group; B, mixture of plasma digests of the adenocarcinoma group; a, 25 mM; b, 50 mM; c,100 mM; d, 150 mM; e, 200 mM; f, 500 mM salt concentration SCX fractions for 2-D μLC-MS/MS analysis.

μLC-MS/MS analyses (a–f) of approximately 2 μg AID-HP tryptic digests corresponding to 0.4 μL original blood plasma sample. The 1-D RP μLC-MS/MS analysis provided approximately 10 000 MS/MS spectra for each sample, and the resultant data were evaluated using a Mascot database search against *H. sapien* subsets of the sequences in the Swiss-Prot database.

In order to achieve statistical confidence levels in identification of proteins from highly complex mixture samples, we investigated the thresholds as filters to extract data for the Mascot peptide score. We used the datasets, obtained from the 1-D μLC-MS/MS analysis with LTQ, of the digested 26S proteasome sample within our search tolerances. Since it is possible to identify several proteins from a single MS/MS spectrum based on the hit sequence varieties, the most significant peptide sequence that was ranked first (marked with bold red in the Mascot search results), which had the highest score among the hit varieties, was extracted from the entire datasets to prevent erroneous identifications and redundancy. The resulting peptide assignments were sorted according to their Mascot peptide score and intergraded into protein identification. Figure 5 (see also Supplementary Table A) shows the relationship between the peptide score ranges and either the number of peptide fragments assigned as 26S proteasome or other proteins identified erroneously. Although peptides with a score less than 50 were assigned to both the 26S proteasome and to the other proteins, all peptide fragments with a score of more than 50 were confidently identified as belonging to the 26S proteasome. For thresholds of peptide scores higher than 20, 30, and 40, the statistical identification confidence levels of the Mascot database search results were 70%, 90%, and 97%, respectively. Accordingly, we tentatively set peptide scores more than 30 and ranked first as the criterion for a broad protein identification index in order to integrate the datasets of the μLC-MS/MS analysis of plasma samples. Furthermore, to extract plasma proteins with a higher confidence level, we finally tried to apply the Swiss-Prot dataset (667 proteins) in a non-redundant list of 1175 distinct proteins that Anderson *et al.* have recently developed by combining four separate sources of human plasma proteome [3, 13–16].

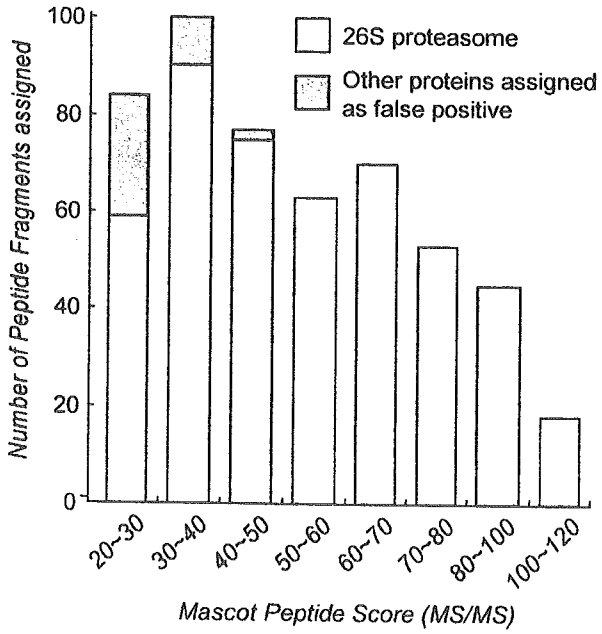


**Figure 5.** Mascot database search results of 1-D μLC-MS/MS analysis of the digested 26S proteasome. See also Supplementary Table A.

The Mascot database search results on plasma proteome analysis yielded data extracted under the thresholds of peptide scores higher than 30 and ranked first; an average of 108 proteins were detected from each 1-D μLC-MS/MS analysis. From the 2-D μLC-MS/MS analysis of the mixture sample of two groups, an average of 249 proteins was assigned as plasma proteome candidates. (Supplementary Table B). Additionally, entire datasets of these Mascot search results were integrated and processed with the data extraction. The results indicated that a total of 506 different proteins were listed, and 180 proteins were detected as common proteins from both groups (Fig. 6, in parentheses). Furthermore, plasma proteins with a high confidence level were extracted from these datasets using the Swiss-Prot dataset of the 667 plasma proteins reported. Figure 6 shows the diagrammatic representation of proteins found in the two groups comprising healthy individuals and adenocarcinoma patients, and the numbers are concordant with the proteins annotated as plasma proteins in 667 Swiss-Prot datasets. The results indicated that 84 and 85 proteins were extracted from the healthy and adenocarcinoma groups, respectively, and 69 proteins were common. In addition, 16 proteins were

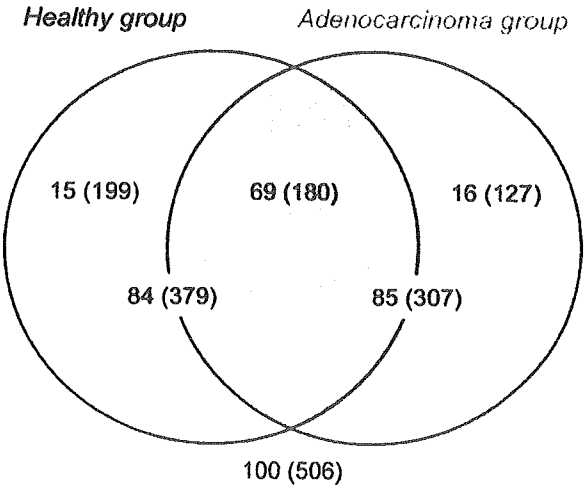


**Figure 6.** Diagrammatic representation of the proteins detected in the groups of healthy individuals and adenocarcinoma patients by 1-D and 2-D μLC-MS/MS analyses of their plasma samples. Numbers that belong to the peptide score thresholds higher than 30 served as the criteria for protein extraction (expressed in parentheses), and the numbers are concordant with the plasma proteins reported in the 667 Swiss-Prot datasets.

**Table 2.** Selected specific protein list of the healthy and lung adenocarcinoma groups in human blood plasma.

| Accession No. | Protein name | Adenocarcinoma plasma samples | | | | | Healthy plasma samples | | | | | |
|---|---|---|---|---|---|---|---|---|---|---|---|---|
| | | 2-D analysis | 1-D μLC-MS/MS analysis | | | | 2-D analysis | 1-D μLC-MS/MS analysis | | | | |
| | | AC8894 | AC88 | AC94 | AC8894-1 | AC8894-2 | H-NIS | H-N | H-I | H-S | H-NIS-1 | H-NIS-2 |
| P02649 | Apolipoprotein E | A | C | A | A | A | | | C | | | |
| Q14624 | Inter-alpha-trypsin inhibitor heavy chain H4 | A | C | B | C | | C | | C | C | C | C |
| P04196 | Histidine-rich glycoprotein | A | | | | | | | | | | |
| P00748 | Coagulation factor XII | B | | | | | | | | | | |
| P00488 | Coagulation factor XIII A chain | B | | | | | C | | | | | |
| P02570 | Actin, cytoplasmic 1 | C | | | | | A | A | C | | C | |
| P27169 | Serum paraoxonase/arylesterase 1 | | | | | | A | | | | | |
| P29312 | 14-3-3 protein zeta/delta | | | | | | | | A | | | |
| P54108 | Cysteine-rich secretory protein-3 | C | | | | | B | | | | | |
| O14791 | Apolipoprotein L1 | | | | | | B | | | | | |
| P02751 | Fibronectin | | | | | | B | | | | | |
| P06396 | Gelsolin, plasma | | | | | | B | | | | | |

Two adenocarcinoma plasma samples (AC88 and AC94) and three healthy plasma samples (H-N, H-I, and H-S) were analyzed by 1-D μLC-MS/MS analysis. The mixture samples separated into both groups (AC8894 and H-NIS) were analyzed twice by 1-D and once by 2-D μLC-MS/MS analysis (2-D analysis). A–C indicated the presence of peptide fragment(s) assigned to the listed protein. A, mascot peptide score higher than 50; B, score 40 to 50; C, score 20 to 40. See also Supplementary Table B.

detected as specific significant proteins of the adenocarcinoma group, and 15 proteins were not detected in the adenocarcinoma group. Table 2 (see also Supplementary Table B) shows a list of the specific proteins assigned by peptide fragment(s) with scores higher than 40. These specific proteins detected from only one group might be candidate biomarkers of lung adenocarcinoma in human blood plasma. However, further statistical verification of our results through data accumulation of more disease plasma samples and the investigation concerning the reproducibility of protein identifications for each sample are necessary. Additionally, validation of these protein identifications by several biochemical approaches would be required. In the present study, we could indicate that several significant protein candidates in the plasma proteome are possibly associated with the pathological differences in lung adenocarcinoma. Functions of specific proteins and their correlations with adenocarcinoma along with the other proteins are not listed in this paper and will be reported elsewhere. These experimental achievements suggest that our automated 1-D and 2-D μLC-MS/MS protein profiling systems, in which the LTQ was incorporated, are powerful in identifying low-abundance proteins of great clinical importance, because these molecules directly report the occurrence and progress of various diseases.

## 4 Concluding remarks

In the course of the Human Plasma Organization Plasma Proteome Project, several research groups have prepared contrast reference specimens of human plasma using various technology platforms [17]. It is extremely important to catalog the plasma proteome as a protein database for clinical plasma proteomics. Applied technology platforms are very powerful, particularly for comprehensive broad protein identification of highly complex samples such as blood plasma. However, it seems difficult to stably and reproducibly apply these to routine clinical investigations that require a large number of proteome analysis runs for a large number of human samples. We have recently established a fully automated, high-throughput 2-D SCX/RP μLC-MS/MS protein profiling system, which can perform large-scale analysis in clinical proteomics [10]. In this study, the LTQ, which is superior to a conventional 3-D ITMS instrument in sensitivity and scan speed, was utilized in our high-throughput system, and it was evaluated by analyzing BSA and human 26S proteasome. Furthermore, the system was applied to plasma proteome analysis in a few cases of both healthy individuals and lung adenocarcinoma patients. The results confirmed that a 10-fold increase in terms of sensitivity was achieved in our system using the LTQ instrument for protein

identification. Further, in comparison with the conventional 3-D ITMS instrument, a three-fold higher number of peptide fragments was identified as belonging to the 26S proteasome, indicating significant improvement in resolution for the analytical time point. Additionally, approximately 250 and 100 different proteins were detected, based on the investigation criterion for a 90% confidence level of protein identification, from only 0.4 μL human plasma using 2-D and 1-D μLC-MS/MS analyses, respectively. The entire operation was automatically carried out within 11 h for both single 1-D and 2-D μLC-MS/MS analyses. From the protein identification datasets of both healthy and adenocarcinoma plasma samples, several disease-specific proteins were found in the human plasma based on the plasma proteome database reported earlier. Consequently, it was demonstrated that our μLC-MS/MS protein profiling system is feasible for large-scale analyses such as clinical plasma proteomics studies. Although plasma proteome analysis for clinical application still remains a great challenge due to the wide dynamic range of protein abundance, we shall continue further technological development of the large-scale proteome analysis based on the high-throughput μLC-MS/MS system reported in this paper. Such high-throughput and large-scale analysis of human plasma would lead to the discovery of new disease-associated protein markers with high sensitivity and high specificity in early disease detection and diagnosis, and this would revolutionize current therapeutics.

*The authors gratefully acknowledge the technical assistance of Ms. Hisae Anyoji and Noriko Araki of Medical Proteoscope, Co. Inc., and medical doctors of the Department of Surgery, Tokyo Medical University, as well as the encouragement and support of AMR Inc., Tokyo, Japan. We are also deeply indebted to Drs. Hiroshi Matsumoto and Masayuki Kubota of Thermo Electron Co., Kanagawa, Japan for their assistance.*

## 5 References

[1] Liotta, L. A., Ferrari, M., Petricoin, E., *Nature* 2003, *425*, 905.

[2] Anderson, N. L., Anderson, N. G., *Mol. Cell. Proteomics* 2002, *1*, 845–867.

[3] Anderson, N. L., Polanski, M., Pieper, R., Gatlin, T. *et al.*, *Mol. Cell. Proteomics* 2004, *3*, 311–326.

[4] Washburn, M. P., Wolters, D., Yates, J. R. III, *Nat. Biotechnol.* 2001, *19*, 242–247.

[5] Wolters, D. A., Washburn, M. P., Yates, J. R., III, *Anal. Chem.* 2001, *73*, 5683–5690.

[6] Shen, Y., Jacobs, J. M., Camp, D. G., II, Fang, R. *et al.*, *Anal. Chem.* 2004, *76*, 1134–1144.

[7] Kawakami, T., Nagata, T., Muraguchi, A., Nishimura, T., *Electrophoresis* 2000, *21*, 1846–1852.

[8] Kawakami, T., Nagata, T., Muraguchi, A., Nishimura, T., *J. Chromatogr. B* 2003, *87*, 223–229.

[9] Fujii, K., Nakano, T., Kawamura, T., Usui, F. *et al.*, *J. Proteome Res.* 2004, *3*, 712–718.

[10] Fujii, K., Nakano, T., Hike, H., Usui, F. *et al.*, *J. Chromatogr. A* 2004, *1057*, 107–113.

[11] Tojo, H., *J. Chromatogr. A* 2004, *1056*, 223–228.

[12] http://www.matrixscience.com

[13] Pieper, R., Su, Q., Gatlin, C. L., Huang, S. T. *et al.*, *Proteomics* 2003, *3*, 422–432.

[14] Adkins, J. N., Varnum, S. M., Auberry, K. J., Moore, R. J. *et al.*, *Mol. Cell. Proteomics* 2002, *1*, 947–955.

[15] Tirumalai, R. S., Chan, K. C., Prieto, D. A., Issaq, H. J. *et al.*, *Mol. Cell. Proteomics* 2003, *2*, 1096–1103.

[16] Pieper, R., Gatlin, C. L., Makusky, A. J., Russo, P. S. *et al.*, *Proteomics* 2003, *3*, 1345–1364.

[17] Omenn, G. S., *Proteomics* 2004, *4*, 1235–1240.

 

# Locally Recurrent Central-Type Early Stage Lung Cancer < 1.0 cm in Diameter After Complete Remission by Photodynamic Therapy*

*Kinya Furukawa, MD, PhD; Harubumi Kato, MD, PhD; Chimori Konaka, MD, PhD; Tetsuya Okunaka, MD, PhD; Jituo Usuda, MD, PhD; and Yoshiro Ebihara, MD, PhD*

***Background:*** **It is well known that central-type early stage lung cancer < 1.0 cm in diameter shows almost 100% complete response (CR) to photodynamic therapy (PDT). However, we have encountered cases of local recurrence after CR of tumors with a surface diameter < 1.0 cm.**
***Patients and methods:*** **Ninety-three patients with 114 lesions were followed up, and cases of recurrence after CR has been obtained with initial tumors that had a diameter < 1.0 cm were examined. We compared the cytologic findings of local recurrence after CR to the cytologic findings before PDT. The relationship between the cell features and the depth of bronchial tumor invasion before PDT and on recurrence was evaluated.**
***Results:*** **The CR and 5-year survival rates of patients with lesions < 1.0 cm were 92.8% (77 of 83 patients) and 57.9%, respectively; meanwhile, in the group of patients with lesions ≥ 1.0 cm, CR and 5-year survival rates were 58.1% (18 of 31 patients) and 59.3%. There was a significant difference in efficacy between the two groups ($p < 0.001$). Recurrences after CR were recognized in 9 of 77 lesions (11.7%) < 1.0 cm. When the recurrent tumor cells showed type I-II (low-to-moderate atypia) at the same site initially treated, CR could be obtained by a second PDT. Type III cells (high-grade atypia) showed the characteristics of tumor cells from deeper layers of the bronchial wall. Local recurrence at the same site may be caused by residual tumor cells from deep layers because of inadequate laser irradiation and penetration.**
***Conclusions:*** **To reduce the recurrence rate, it is essential to accurately grasp the tumor extent and the depth of the bronchogenic carcinoma before performing PDT. Analysis of cell features of recurrent lesions after CR appears to be a useful source of information as to the depth of cancer invasion in the bronchial wall.** ***(CHEST 2005; 128:3269–3275)***

**Key words:** early stage lung cancer; occult lung cancer; photodynamic therapy; porfimer sodium

**Abbreviations:** AFB = autofluorescence bronchoscopy; CIS = carcinoma *in situ*; CR = complete remission; EBUS = endobronchial ultrasonography; ESLC = early stage lung cancer; PDT = photodynamic therapy; PR = partial remission

Lung cancer has a tendency to develop in older people, with a very poor prognosis. A total of 55,000 Japanese died from lung cancer in 2003, which made it the number-one cause of cancer death. Although diagnostic techniques such as high-resolution CT scan, video bronchoscopy, fluorescence bronchoscopy, and endobronchial ultrasonography (EBUS) have been developed recently, many patients with newly detected lung cancer still have inoperable advanced cancer. Therefore, the detection of early stage lung cancer (ESLC) is considered essential to reduce the mortality rate. Meanwhile, even when ESLC is detected, some cases are inoperable because of cardiopulmonary dysfunction due to age. Endoscopic procedures that are minimally invasive and do not compromise pulmonary function

*From the Department of Chest Surgery (Dr. Furukawa), Kasumigaura Hospital, Tokyo Medical University, Ibaraki; First Department of Surgery (Drs. Kato, Konaka, Usuda, and Ebihara), Second Department of Pathology, Tokyo Medical University, Tokyo; and Center for Respiratory Diseases (Dr. Okunaka), Sanno Hospital, Tokyo, Japan.
Manuscript received February 12, 2005; revision accepted May 9, 2005.


*Correspondence to: Kinya Furukawa, MD, PhD, Department Chest Surgery, Tokyo Medical University, Kasumigaura Hospital, 3-20-1 Chuo, Ami-machi, Inashiki-gun, Ibaraki 300-0395, Japan; e-mail: k-furu@tokyo-med.ac.jp*

are considered useful modalities for centrally located lung cancer. In particular, photodynamic therapy (PDT) is considered a useful and attractive modality for central-type ESLC.[1–7] Its action mechanism is considered to involve singlet oxygen, which is generated through photochemical reactions and causes degenerative necrosis of cells that have taken up the photosensitizer, *ie*, tumor cells.[8]

PDT using red laser light and a tumor-specific photosensitizer was established as a new therapeutic modality for central-type ESLC in 1982.[1] The length of longitudinal tumor extent was the only independent predictive factor for complete remission (CR), and 100% CR in lesions < 1.0 cm in diameter treated by PDT was reported.[5] However, we have encountered local recurrences after CR of tumor even in cases with a surface diameter < 1.0 cm. Therefore, we investigated the characteristics and cytomorphologic features of primary lesions and recurrences after CR in patients with lesions < 1.0 cm in diameter.

## Materials and Methods

### *Patient Selection*

A total number of 145 patients with 191 lesions of endoscopic ESLC underwent PDT from February 1980 to April 2001 in the Department of Tokyo Medical University. Of the 145 patients with 191 lesions, 93 patients with 114 lesions were followed up, and cases of recurrence after CR was obtained with initial tumors with a diameter < 1.0 cm were examined.

### *Procedures of PDT and Follow-up*

The depth of tumor invasion was judged by biopsy specimen and CT scan, and was also evaluated by bronchoscopic findings based on the diagnostic criteria of ESLC defined by the Japan Lung Cancer Society.[9] To determine tumor size, bronchoscopic biopsies of the proximal and distal sites of the lesion and bronchoscopic measurements using forceps were performed. PDT procedures were performed with the combination of porfimer sodium (Photofrin; Wyeth Japan K.K.; Tokyo, Japan) that is taken up selectively in tumor, and an argon gas laser system (model 770; Spectra-Physics; Mountain View, CA) or excimer dye laser (EDL-1; Hamamatsu Photonics; Hamamatsu, Japan). Laser irradiation was performed via a quartz fiber inserted through the biopsy channel of the endoscope at 48 h after the IV administration of 2.0 mg/kg of porfimer sodium. The total energy of the laser irradiation was 100 J/cm$^2$, and energy levels in this range do not cause any heat degeneration or other adverse effects. The duration of irradiation required usually 10 to 20 min. Clean-up bronchoscopies to remove necrotic tissue produced by the PDT reaction were performed at 1, 3, and 7 days after PDT. Both cytologic and histologic examinations via fiberoptic bronchoscopy were performed at 1, 2, and 3 months, and thereafter at 3-month intervals in the first year and 6-month intervals after the second year until 5 years after PDT.

### *Efficacy Evaluation*

The antitumor effect of initial treatment was rated based on endoscopic measurement of tumor size using forceps, morphologic observations, and histopathologic examination by biopsy, according to the general rules of the Japan Lung Cancer Society[9] and the Japan Society of Clinical Oncology.[10] The antitumor effect was rated at 1 month and 2 months after PDT. Antitumor effect was rated as CR (no demonstrable tumor microscopically by brushing and/or biopsy for a period of 4 weeks), partial remission (PR) [≥ 50% reduction in tumor size], no change (< 50% reduction or < 25% increase in tumor size), progressive disease (> 25% increase in tumor size), or not evaluable.

### *Evaluation of Cytomorphologic Features of Local Recurrences*

In the central-type ESLC < 1.0 cm in greatest dimension, we have compared the cytologic findings of local recurrence after CR to the cytologic findings before PDT using bronchial brushing specimen. Cytologic findings were classified into three cytologic morphotypes using the classification of cell features proposed by Konaka and coworkers,[11] which appears to yield information as to the depth of cancer invasion in the bronchial wall. The classification was described as follows: type I cell, low-grade atypia (resembling atypical squamous cell metaplasia); type II cell, moderate-grade atypia (resembling early stage squamous cell carcinoma); and type III cell, high-grade atypia (resembling invasive squamous cell carcinoma). The biopsy specimens before PDT and on recurrence, or resected materials, in cases of resection after recurrence, were examined histopathologically, and the depth of bronchial wall invasion was classified into three groups: grade 1, carcinoma *in situ* (CIS) or microinvasion; grade 2, extramuscular bronchial wall invasion; and grade 3, intracartilaginous to extracartilaginous invasion. The relationship between the cell features and the depth of bronchial tumor invasion before and after PDT was evaluated.

### *Statistical Analysis*

Statistical analysis were done using statistical software (Stat Flex for Windows, version 5.0; Artec; Osaka, Japan). The $\chi^2$ test was used to compare the efficacy of PDT between lesions < 1.0 cm and > 1.0 cm in diameter. Differences between the survival rates of two groups in the Kaplan-Meier survival curves were analyzed using the log-rank test; $p < 0.05$ was considered to indicate a statistically significant difference.

## Results

### *Results of PDT for Central-Type ESLC*

A total of 93 patients with 114 lesions of central-type ESLC who underwent PDT were examined. Thirteen synchronous lesions in six cases, 15 metachronous lesions in six cases, and 5 synchronous/metachronous lesions in one case were observed. The evaluation of the efficacy of PDT is shown in Table 1. CRs and PRs were obtained in 75 patients with 95 lesions (83.3%) and in 18 patients with 19 lesions (16.7%) out of 93 patients with 114 lesions. Each lesion with PR was subsequently treated with other modalities, including surgery in 13 cases, chemotherapy in 5 cases, or radiotherapy in 1 case, and finally achieved 100% CR. Recurrences after CR were recognized in 12 of 95 lesions (12.6%). The 114 lesions were classified in two groups according to the

**Table 1—*Results of PDT for Central-Type ESLC**

| Tumor Size, cm | Lesions, No. | CR | PR | Recurrence After CRT |
|---|---|---|---|---|
| < 1.0 | 83 | 77 (92.8) | 6 (7.2) | 9 (11.7) |
| ≥ 1.0 | 31 | 18 (58.1) | 13 (41.9) | 3 (16.7) |
| Total | 114 | 95 (83.3) | 19 (16.7) | 12 (12.6) |

*Data are presented as No. (%) unless otherwise indicated.
†p < 0.001.

maximum longitudinal tumor extent. Of these, 83 lesions (72.8%) were < 1.0 cm and 31 lesions (27.2%) were ≥ 1.0 cm in diameter. The CR and PR rates in the group of patients with lesions < 1.0 cm in maximum diameter were 92.8% (77 of 83 patients) and 7.2% (6 of 83 patients), respectively. Meanwhile, in the group of patients with lesions ≥ 1.0 cm in diameter, the CR and PR rates were 58.1% (18 of 31 patients) and 41.9% (13 of 31 patients), respectively. Neither no change nor partial disease were observed in these groups. There was a significant difference in efficacy between the two groups using the $\chi^2$ test ($p < 0.001$). Recurrences after CR were recognized in 9 of 77 lesions (11.7%) in the group < 1.0 cm and 3 of 18 lesions (16.7%) in the group ≥ 1.0 cm in diameter. The overall 5-year survival rates of the two groups were 57.9% and 59.3%, respectively (Fig. 1). There was no significant difference between the two groups on the basis of the log-rank test ($p = 0.207$).

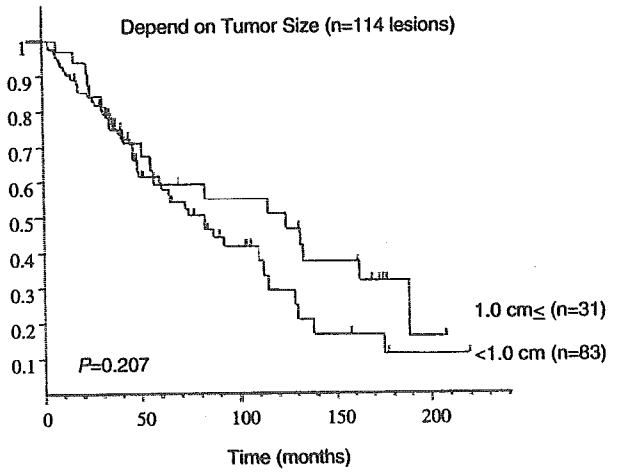


FIGURE 1. The overall 5-year survival rates were 57.9% in the group of patients with tumors < 1.0 cm and 59.3% in the group with tumors ≥ 1.0 cm in diameter, respectively. There was no significant difference between the survival rates of two groups in the Kaplan-Meier curves on the basis of the log-rank test ($p = 0.207$).

### *Characteristics of Local Recurrence < 1.0 cm in Diameter After CR*

The information on nine patients with nine lesions in the group of patients with lesions < 1.0 cm in diameter who had recurrence after CR had been achieved by initial PDT are presented in Table 2. All patients with recurrence were male, and the age distribution ranged from 64 to 71 years (average age, 67.6 years at the time of initial diagnosis). Evidences of local recurrence were found in nine patients with nine lesions at the site of the primary lesion. The recurrent lesions were located on the trachea in one patient, lobar bronchus in one patient, segmental bronchi in five patients, and subsegmental bronchi in two patients. The average diameter of the nine recurrent lesions was 0.46 cm. All lesions were squamous cell carcinoma, and endoscopic findings showed nodular type in two lesions and superficial type in seven lesions. The disease-free interval of these nine patients ranged from 3 to 18 months (average, 10 months).

Local recurrence at site corresponding to the

**Table 2—*Recurrent Cases After PDT for Central-Type ESLC < 1.0 cm in Diameter**

| Case No. | Patient Age, yr | Lesion | Size, cm | BF Findings | CR, mo | Recurrence | Additional Treatment | Prognosis |
|---|---|---|---|---|---|---|---|---|
| 1 | 66 | Segmental bronchus $rB^3$ | 0.3 | Superficial | 18 | PM | PDT, OP (RUL) | Alive (24 mo) |
| 2 | 64 | Subsegmental bronchus $IB^3$ a-b | 0.3 | Superficial | 13 | PM | PDT, OP (LPn) | Dead (56 mo), other disease |
| 3 | 69 | Subsegmental $rB^{10}$ a-b | 0.4 | Superficial | 10 | PM | PDT Brachy | Alive (41 mo) |
| 4 | 64 | Segmental bronchus $IB^{1+2}$ | 0.6 | Nodular | 5 | SS (CIS) | PDT | Alive (24 mo) |
| 5 | 66 | Segmental bronchus $rB^1$ | 0.5 | Superficial | 3 | SS (CIS) | | Dead (5 mo), other disease |
| 6 | 69 | Segmental bronchus $IB^{1+2}$ | 0.4 | Superficial | 14 | SS (CIS) | PDT | Alive (27 mo) |
| 7 | 71 | Trachea | 0.3 | Nodular | 10 | SS (CIS) | PDT | Alive (27 mo) |
| 8 | 70 | Lobar bronchus rMid.-low | 0.9 | Superficial | 6 | SS (intracartilage) | OP (RML) | Dead (56 mo), other disease |
| 9 | 69 | Segmental $IB^{1+2}$ $B^3$ | 0.4 | Superficial | 11 | SS (extracartilage) | Nd-YAG, radiation, OP | Alive (65 mo) |

*PM = peripheral margin initially treated; SS = same site initially treated; OP = operation; RML = right middle lobe; RUL = right upper lobe; LPn = left pneumonectomy; BF = bronchofiberscopic.

Table 3—*Cell Feature and Depth of Bronchial Invasion*

| Case No. | Before PDT | | Recurrence | |
|---|---|---|---|---|
| | Cytology (Brush) Type | Pathologic Grade | Cytology (Brush) Type | Pathologic Grade |
| 4 | I | 1 | I | 1 |
| 5 | I | 1 | I | 1 |
| 6 | I–II | 1 | I–II | 1 |
| 7 | I | 1 | II | 1 |
| 8 | I–II | 1 | II–III | 3 (intracartilaginous invasion) |
| 9 | I | 1 | III | 3 (extracartilaginous invasion) |

peripheral margin of the lesion initially treated by PDT was observed in three patients (cases 1 to 3), while local recurrence at the same site as the initial tumor initially treated was observed in six patients (cases 4 to 9). The local recurrences at the site corresponding to the peripheral lesion were initially located in the subsegmental bronchus in two of three primary lesions. The patients with three local recurrences at the site corresponding to the peripheral margin underwent a second PDT session; however, CR was not obtained in any of these patients. Therefore, additional conventional surgery was performed in two patients and brachytherapy in one patient. The pathologic examinations of two operated patients showed residual tumor at the peripheral site. Right upper lobectomy was performed for case 1, and the resected material revealed superficial tumor invasion peripheral to the right $B^3b$. Left pneumonectomy was selected for case 2 (ipsilateral double cancer) because an ESLC was located at the bifurcation of left $B^3a$-b and a malignant lymphoma was in left $B^6$. This patient died due to malignant lymphoma at 56 months after the initial PDT session. Four patients (cases 4 to 7) with six local recurrences at the same site as the initial tumor local showed superficial tumor invasion (CIS), and a second PDT session was performed in three of four patients. CRs were again obtained in all three patients, who are presently disease free. One double cancer patient who had advanced stomach cancer underwent systemic chemotherapy without a second PDT but died 5 months after the initial PDT session. The pathologic examinations of the two other surgically treated patients (cases 8 and 9) revealed intracartilagious invasion of the bronchial wall. One multiple lung cancer patient (case 8) who received right middle and lower lobectomy after local recurrence died of hemoptysis due to another advanced lung cancer at 56 months after the initial PDT session. At the last follow-up of the nine patients who had local recurrence after CR had been obtained by initial PDT in whom the original primary lesion had been < 1.0 cm

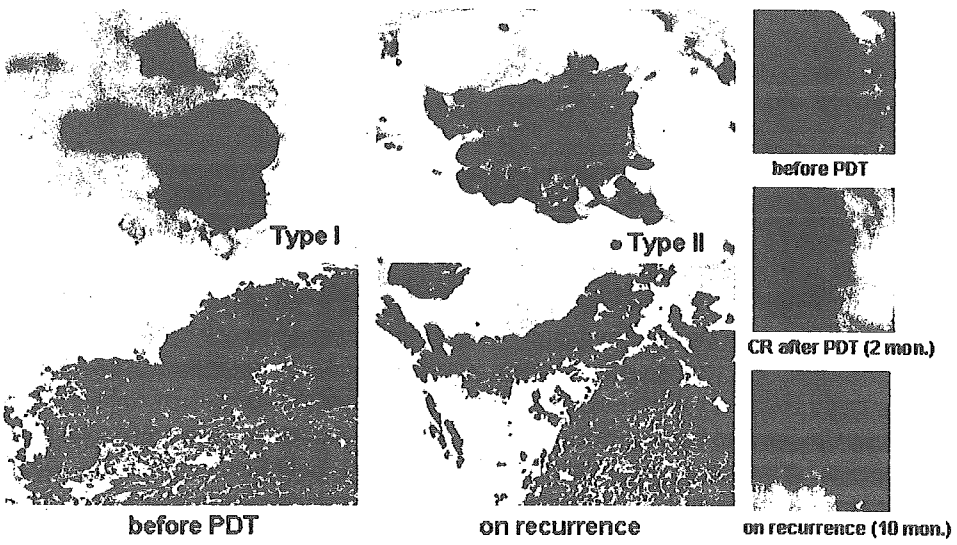


FIGURE 2. The cytopathologic and bronchoscopic findings in case 7. Bronchoscopic findings showed a small nodular tumor at the right side of the tracheal wall before PDT. Redness of the tracheal mucosa was observed on recurrence at 10 months after PDT. Cytologic findings before PDT were classified as type I because cell features showed a round shape and slight increase of nuclear chromatin but low-grade nuclear atypia. The biopsy specimen showed CIS (grade 1). Cytologic findings on recurrence were classified as type II because a sheet formation of polymorphic-shaped cells, increase of nuclear chromatin, and nuclear body were observed. Biopsy specimen on recurrence showed superficial tumor invasion (CIS) beneath the thin epithelial layer (grade 1). A second PDT was performed, and CR was again obtained in this patient.

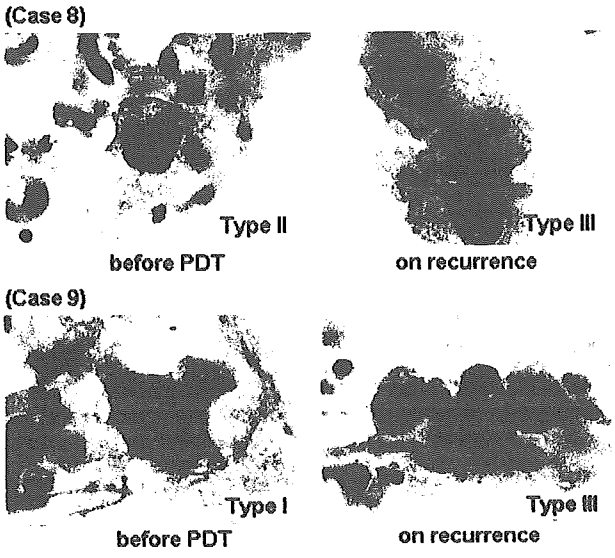


FIGURE 3. The findings of brushing cytology mainly observed in cases 8 and 9 before PDT and on recurrence after CR. Cytologic findings before PDT in case 8 were classified as type II because of a slight increase of nuclear chromatin. Cytologic findings before PDT in case 9 were classified as type I because of low-grade nuclear atypia. The findings of recurrent tumor cells in cases 8 and 9 were classified as type III because of severe increases of nuclear chromatin, high nuclear/cytoplasmic ratio, and high grade of nuclear atypia.

in diameter, three patients had died of other diseases and six patients were alive, and there were no deaths from the primary lesion.

### *Evaluation of Cytomorphologic Features of Local Recurrences*

As mentioned above, local recurrence of the carcinoma at the same site as lesions < 1.0 cm in diameter initially treated successfully by PDT was observed in six out of nine locally recurrent patients (cases 4 to 9). A summary of the cell features and depth of bronchial wall invasion before PDT and after recurrence are shown in Table 3. The brushing cytology specimens before PDT mainly showed type I or II, and biopsy revealed grade 1 in all six cases. The majority of cell features in cases 4 to 7 showed type I or II, and the biopsy specimens showed grade 1 on recurrences. The cytopathologic and bronchoscopic findings of case 7 are shown Figure 2. Populations of type I and II cells were predominant in the recurrent lesions in these cases, which implied that the recurrent tumor was located in a superficial layer of bronchial wall. When the recurrent tumor cells showed type I-II (low-to-moderate atypia) local recurrence at the same site as the initial tumor initially treated, CR could be obtained by a second PDT. In cases 8 and 9, mainly type III cell features were observed in brushing cytology on recurrence (Fig 3). These two cases underwent resection, and the resected specimens revealed intracartilaginous tumor invasion of bronchial wall (grade 3), which implied the residual tumor located in a deep layer of bronchial wall.

## DISCUSSION

PDT for cancer using a combination of low-power laser irradiation and tumor specific photosensitizer was first applied clinically by Dougherty et al[12] in 1978 to the skin metastasis of breast cancer. Since then, we performed the first reported endoscopic clinical application of PDT in cooperation with Dougherty and coworkers.[12] In Japan, PDT using porfimer sodium, a tumor-specific photosensitizer and excimer dye laser, was recognized by the government; and from April 1996, hospitals could receive reimbursement for PDT of early stage carcinomas of the lung, esophagus, stomach, and cervix from the national health insurance system.

The best PDT candidates in lung cancer are cases with central-type ESLC because of their endoscopic accessibility; therefore, selection of patient is important to achieve CR. Nagamoto et al[13] demonstrated that no lymph node involvement was found in 59 cancers with a longitudinal extent of < 20 mm; in another study,[14] histology by serial block sectioning showed that there was no nodal involvement in any CIS cases. Nakamura et al[15] retrospectively analyzed resected cases of central-type ESLC to clarify the relation between the endoscopic findings and the histologic extent of tumor. They demonstrated a significant difference is the maximum dimension according to the depth of bronchial invasion between CIS and extramuscular invasion and CIS and invasion into or beyond the cartilaginous layer. Lesions with a maximum diameter < 1.0 cm have a high possibility of being CIS. Their preoperative bronchoscopic diagnosis of centrally located ESLC was correct in 74.0%. In another study, Akaogi et al[16] demonstrated that polypoid or nodular lesions < 1.0 cm and flatly spreading lesions < 1.5 cm in greatest dimension were limited to within the cartilaginous layer without regional lymph node involvement. Also, Furuse et al[5] demonstrated that the length of longitudinal tumor extent was the only independent predictive factor for CR by PDT, and that lesions < 1.0 cm in diameter showed 100% CR. According to these data, therapy for CR requires satisfaction of the following endoscopic conditions: (1) no evidence of lymph node metastasis; (2) the lesion is superficial with a maximum diameter of < 1.0 cm; (3) no invasion into or beyond the cartilaginous layer; (4) the histologic type is squamous cell carcinoma; and

(5) the lesion is located in a position that can be easily irradiated with the laser.

In this study, excellent efficacy with a significant difference of CR rate was seen in patients with lesions $< 1.0$ cm (92.8%) compared to $\geq 1.0$ cm (58.1%) in diameter; however, the overall 5-year survival rate of the two groups showed no significant difference (57.9% vs 59.3%). This may be because it was possible to perform additional alternative modalities such as surgery, second PDT, and brachytherapy to achieve CR after failure of initial PDT or recurrence after PDT. Considering that the 5-year survival rate of pathologic stage Ia (T1N0M0) patients who underwent surgery is approximately 67.0%,[17] our data are favorable because the majority of the PDT group consisted of patients with advanced age and poor cardiopulmonary function. Therefore, we consider that PDT may be used as first-line therapy for central-type ESLC prior to surgery, especially in cases with poor cardiopulmonary function. Also, Edell et al[18] and Cortese et al[19] demonstrated that PDT is an alternative to surgical resection in the management of early superficial squamous cell carcinoma.

In this study, recurrence after CR was recognized in 9 of 77 lesions (11.7%) in the group of patients with lesions $< 1.0$ cm in diameter. Despite the average diameter of the nine initial lesions being relatively small (0.46 cm), recurrence was recognized in eight of nine lesions (88.9%) within 12 months. Therefore, intensive follow-up studies should be performed until 1 year after PDT even for small primary lesions. The reasons why recurrences after CR were observed in the lesions $< 1.0$ cm in diameter could be explained by inappropriate estimation of the peripheral margin in cases of local recurrence at the site corresponding to the peripheral margin and insufficient laser irradiation or miss estimation of tumor depth in the cases of local recurrence at the same site as the initial tumor.

From our experiences, to achieve CR with PDT for central-type ESLC, it appears that not only the analysis of cell features but also the comprehension of tumor extent to the peripheral site and tumor invasion to the bronchial wall are of considerable significance. Kurimoto et al[20] demonstrated that endobronchial EBUS was useful to determine the depth of tumor invasion into the bronchial wall, and the accuracy of EBUS from the histopathologic findings was 95.8%. The EBUS image at 20 MHz shows five layers in the cartilaginous portion of bronchial wall. The third to fifth layers are images of cartilage. Therefore, it is feasible to evaluate the depth of invasion using EBUS whether or not the tumor invades into or beyond the cartilaginous layer.. In lesions with an intact third layer on EBUS, CR could be achieved with PDT. Miyazu et al[21] demonstrated that the depth of tumor invasion estimated by EBUS was accurate by histopathologic findings after surgical resection. They found 5 of 14 lesions (35.7%) $< 1.0$ cm in diameter that showed extracartilaginous invasion on the EBUS image that was later confirmed histopathologically; also, 3 of 5 lesions appeared bronchoscopically superficial but were shown to be extracartilaginous by EBUS. The indications of PDT for centrally located ESLC with a longitudinal extension of $< 1.0$ cm are unquestionable; meanwhile, we should realize that even $< 1.0$ cm in diameter can have extracartilaginous invasion. To comprehend the surface extent of superficial tumor invasion in the bronchial lumen, autofluorescence bronchoscopy (AFB) is considered useful.[22–25] The green autofluorescence of the lesion was decreased because of the lack of endogenous fluorophors, thickening of the membrane, and increased microvasculature.[26] We sometimes encountered unexpected surface invasion by AFB.

It is essential to know the extent of the tumor and the depth of bronchogenic carcinoma accurately for the selection of treatment modality. Corresponding to the previous study by Konaka et al,[11] the analysis of cell features is a useful source of information to evaluate the depth of cancer invasion in the bronchial wall. In addition, we believe that it could be beneficial information when choosing the treatment modality, such as recurrence after CR by PDT demonstrated in our study. Additionally, we now perform EBUS and AFB to determine the indications of PDT in all patients who have ESLC for the purpose of achieving 100% CR and reduction of recurrence rate. A comparative study of PDT for the treatment of ESLC before and after the adoption of EBUS and AFB will enable accurate evaluation of the benefits of these new diagnostic tools in the near future.

ACKNOWLEDGMENT: The authors are indebted to Professor J. P. Barron of the International Medical Communications Center of Tokyo Medical University for his review of this article.

## REFERENCES

1 Hayata Y, Kato H, Konaka C, et al. Hematoporphyrin derivative and laser photoradiation in the treatment of lung cancer. Chest 1982; 81:269–277
2 Kato H, Konaka C, Kawate N, et al. Five-year disease-free survival of a lung cancer patient treated only by photodynamic therapy. Chest 1986; 90:768–770
3 Edell ES, Cortese DA. Bronchoscopic phototherapy with hematoporphyrin derivative for treatment of localized bronchogenic carcinoma: a 5-year experience. Mayo Clin Proc 1987; 62:8–14
4 Edell ES, Cortese DA. Bronchoscopic localization and treatment of occult lung cancer. Chest 1989; 96:919–921
5 Furuse K, Fukuoka M, Kato H, et al. A prospective phase II

study on photodynamic therapy with Photofrin II for centrally located early-stage lung cancer. J Clin Oncol 1993; 11:1852–1187
6 Kato H. Photodynamic therapy for lung cancer: a review of 19 years' experience. J Photochem Photobiol 1998; B42:96–99
7 Kato H, Furukawa K, Sato M, et al. Phase II clinical study of photodynamic therapy using mono-L-aspartyl chlorin e6 and diode laser for early superficial squamous cell carcinoma of the lung. Lung Cancer 2003; 42:103–111
8 Niedre M, Patterson MS, Wilson BC. Direct near-infrared luminescence detection of singlet oxygen generated by photodynamic therapy in cells *in vitro* and tissues *in vivo*. Photochem Photobiol 2002; 75:382–391
9 General rules for clinical and pathological records of lung cancer. 4th ed. In: Japan Lung Cancer Society, eds. Tokyo, Japan: Kanehara and Company, 1995; 123–133
10 Niiya H. Toxicity grading criteria of the Japan Clinical Oncology Group. Int J Clin Oncol 1997; 32:61–65
11 Konaka C, Miura H, Ikeda N, et al. The characteristics of early bronchogenic carcinoma evaluated by cytomorphological features. Lung Cancer 2002; 38:267–271
12 Dougherty TJ, Lawrence G, Kaufman JH, et al. Photoradiation in the treatment of recurrent breast carcinoma. J Natl Cancer Inst 1978; 62:231–237
13 Nagamoto N, Saito Y, Ohta S, et al. Relationship of lymph node metastasis to primary tumor size and microscopic appearance of roentgenographically occult lung cancer. Am J Surg Pathol 1989; 13:1009–1013
14 Nagamoto N, Saito Y, Sato M, et al. Clinicopathological analysis of 19 cases of isolated carcinoma in situ of the bronchus. Am J Surg Pathol 1993; 17:1234–1243
15 Nakamura H, Kawasaki N, Hagiwara M, et al. Endoscopic evaluation of centrally located early squamous cell carcinoma of the lung. Cancer 2001; 91:1142–1147
16 Akaogi E, Ogawa I, Mitsui K, et al. Endoscopic criteria of early squamous cell carcinoma of the bronchus. Cancer 1994; 74:3113–3117
17 Mountain CF. Revisions in the international system for staging lung cancer. Chest 1997; 111:1710–1717
18 Edell ES, Cortese DA. Photodynamic therapy in the management of early superficial squamous cell carcinoma as an alternative to surgical resection. Chest 1992; 102:1319–1322
19 Cortese DA, Edell ES, Kinsey JH. Photodynamic therapy for early stage squamous cell carcinoma of the lung. Mayo Clin Proc 1997; 72:595–602
20 Kurimoto N, Murayama M, Yoshioka S, et al. Assessment of usefulness of endobronchial ultrasonography in determination of depth of tracheobronchial tumor invasion. Chest 1999; 115:1500–1506
21 Miyazu Y, Miyazawa T, Kurimoto N, et al. Endobronchial ultrasonography in the assessment of centrally located early-stage lung cancer before photodynamic therapy. Am J Respir Crit Care Med 2002; 165:832–837
22 Lam S, Kennedy T, Unger M, et al. Localization of bronchial intraepithelial neoplastic lesions by fluorescence bronchoscopy. Chest 1998; 113:696–702
23 Ikeda N, Hiyoshi T, Kakihana M, et al. Histopathological evaluation of fluorescence bronchoscopy using resected lungs in cases of lung cancer. Lung Cancer 2003; 41:303–309
24 Sutedja TG, Codrington H, Risse EK, et al. Autofluorescence bronchoscopy improves staging of radiographically occult lung cancer and has an impact on therapeutic strategy. Chest 2001; 120:1327–1332
25 Sutedja TG, Venmans BJ, Smit EF, et al. Fluorescence bronchoscopy for early detection of lung cancer: a clinical perspective. Lung Cancer 2001; 34:157–168
26 Furukawa K, Ikeda N, Miura T, et al. Is autofluorescence bronchoscopy needed to diagnose early bronchogenic carcinoma? J Bronchol 2003; 10:64–69

Journal of Surgical Research 123, 245–250 (2005)
doi:10.1016/j.jss.2004.08.019

# Microwave Coagulation Therapy in Canine Peripheral Lung Tissue[1]

Kinya Furukawa, M.D., Ph.D.,*,[2] Toyoaki Miura, M.D., Ph.D.,* Yasuhumi Kato, M.D.,† Shinya Okada, M.D., Ph.D.,‡ Hidemitsu Tsutsui, M.D., Ph.D.,† Hideaki Shimatani, M.D., Ph.D.,† Naohiro Kajiwara, M.D., Ph.D.,† Masahiro Taira, M.D.,* Makoto Saito, M.D., Ph.D.,* and Harubumi Kato, M.D., Ph.D.†

*Department of Thoracic Surgery, Kasumigaura Hospital, Tokyo Medical University, 3-20-1 Chuo Ami-machi, Inashiki-gun, Ibaraki 300-0395, Japan; †First Department of Surgery, Tokyo Medical University, 6-7-1 Nishi-shinjuku, Shinjuku-ku, Tokyo, Japan; ‡Second Department of Pathology, Tokyo Medical University, 6-7-1 Nishi-shinjuku, Shinjuku-ku, Tokyo, Japan

Submitted for Publication May 9, 2004

***Background.*** **New modalities for local treatments that destroy tumor effectively but which are less invasive and less damaging to normal lung tissue must be developed for patients who are unable to undergo even video-assisted thoracic surgery (VATS) due to poor cardiopulmonary function, severe adhesion, or advanced age, etc. We evaluated the use of microwave coagulation therapy (MCT), which has been used successfully for coagulation of hepatic tumors, in normal canine lung tissue to evaluate its efficacy and safety.**

***Materials and methods.*** **Measurements of thermal response and coagulation area and histological examinations after microwave coagulation were performed in normal canine lung tissue.**

***Results.*** **The temperature in normal canine lung tissue increased to 90–100°C at 5 mm from the electrode after 60 s and 70–80°C at 10 mm after 90 s at 40 or 60 W. The coagulation area was approximately 20 mm in diameter at 40 W and 60 W. Histological analysis demonstrated thickening of collagen fiber shortly after coagulation, stromal edema and granulation tissue after 3 months, and, finally, scar tissue was seen after 6 months.**

***Conclusions.*** **Microwave coagulation therapy (MCT) is a useful modality for minimally invasive therapy in peripheral lung tumors.** 

***Key Words:*** **microwave coagulation; MCT, PMCT, ablation; lung tumor; peripheral lung cancer.**

## INTRODUCTION

Recently, the problem of population aging on a global scale is calling for minimally invasive therapies providing good quality of life (QOL) and activity of daily living (ADL). Many investigators are looking into the problems of poor cardiopulmonary function as a result of advanced age, previous surgery, and/or synchronous or metachronous carcinoma. Meanwhile, the detection rate of early-stage carcinoma or precancerous lesions has increased due to recent advances in medical technology. In the field of chest diseases, the detection rate of tiny tumors in the peripheral lung, such as early-stage lung cancer, small metastases, or atypical adenomatous hyperplasia (AAH) has increased with the increasing use of high-resolution CT scans. Video-assisted thoracic surgery (VATS) usually is used for many of these cases. However, we believe that less-invasive therapy is necessary for patients who are inoperable due to poor cardiopulmonary function, severe adhesion, or advanced age.

There is, therefore, a need for local treatment that effectively destroys tumor but is minimally invasive and less damaging to normal tissue than surgery. In the present study, we focused on microwave coagulation therapy (MCT), which has successfully been used to coagulate hepatic tumors [1–4]. The mechanism of coagulation is dielectric heating, *i.e.*, frictional heat of water molecules. Since the dielectric heat energy cannot be generated in the presence of air, selective tumor damage may be achieved and damage to the surrounding normal air-filled lung tissue may be limited. To assess the application of PMCT for lung tumors, we evaluated its efficacy and safety in experimental studies.

[1] The authors wish to thank Assistant Professor R. Breugelmans and Professor J. P. Barron of the International Medical Communications Center of Tokyo Medical University for their support in reviewing this manuscript.

[2] To whom correspondence and reprint requests should be addressed at Department of Thoracic Surgery, Tokyo Medical University, Kasumigaura Hospital, 3-20-1 Chuo, Ami-machi, Inashiki-gun, Ibaraki 300-0395, Japan. E-mail: k-furu@tokyo-med.ac.jp.



0022-4804/05 $30.00

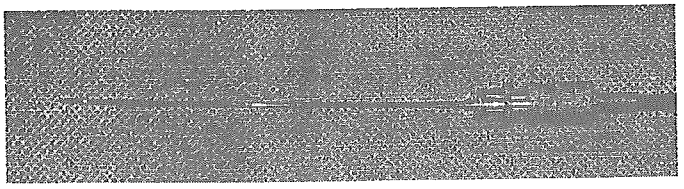

FIG. 1. A specially designed single-needle electrode, 150 mm in length and 1.6 mm in diameter, was inserted 20 mm into the normal lung.

## MATERIALS AND METHODS

### Measurements of Thermal Response

Animal studies were performed with the approval of the Institutional Committee for Ethical Research Animal Care. Adult beagles (10-15 kg) were given artificial respiration under general anesthesia with 30 mg/kg of phentobarbital sodium intravenously and placed in the left lateral recumbent position. Using an aseptic technique, thoracotomy was performed through the 5th intercostal space. A specially designed single-needle electrode (MD-16CBT-10/150, Azwell, Osaka, Japan, Fig. 1) that is 150 mm in length and 1.6 mm in diameter was inserted 20 mm into the normal lung. Then, tissue coagulation was performed using a microwave generator (Microtaze HSD-20W, Azwell, Fig. 2) that emitted 2450 MHz microwaves of 12 cm wavelength at a power output of 20, 40, and 60 W for 4 min. Temperature change was continuously monitored for 4 min using a K-type electric thermometer at 5 mm and 10 mm from the electrode with a sensor inserted 10 mm into the normal lung. The data of temperature were plotted for every 15 s. Measurements of temperature change were performed three times in each condition. Three beagles were used for this study.

### Measurements of Coagulation Area

Microwave electrodes were inserted into normal lung tissue of beagles using the same procedure as mentioned above. Microwave coagulation was performed three times under each condition at power outputs of 20, 40, and 60 W for 1, 2, 3, and 4 min. Three beagles were used for this study. Shortly after microwave coagulation, the beagles were euthanized with an intravenous phentobarbital sodium overdose and pneumonectomy was performed. The resected canine lungs were inflated with bubbling air and 10% buffered formalin from the bronchial stump using an enema syringe pump and preserved in 10% buffered formalin for tissue fixation.

Under the same conditions, microwave coagulation was performed for normal human fresh lung tissue after resection of central type lung carcinoma, inflated with bubbling air using an enema syringe pump from the bronchial stump. Coagulation was performed once under each condition using two fresh lung lobes after resections. Informed consent was obtained in all cases. Tissue fixation was performed in the same manner as in the animal experiment.

The fixed lung tissue was transected perpendicular to the direction of the inserted electrode. The longest dimension of the maximum coagulation area of fixed lung tissue was measured.

### Histological Examinations after Microwave Coagulation

Microwave coagulations were performed in three beagles at a power output of 40 W for 3 min. One beagle was euthanized with an intravenous phentobarbital sodium overdose immediately, and the other two beagles were followed up to assess histological change of the coagulated tissue. The normal activity and condition of each beagle was monitored daily. These beagles were euthanized at 3 and 6 months after the procedure. Histological changes of normal lung tissue immediately, 3 and 6 months after microwave coagulation were investigated by H-E staining and Elastica von Gieson staining.

### Statistical Analysis

Data were expressed as means ± standard deviations (SD), and statistical analyses were done using Student's $t$ test with computer software (Microsoft Excel, version 2002). A $P$ value of less than 0.05 was considered to indicate a statistically significant difference.

## RESULTS

### Measurements of Thermal Response

The data of thermal response of normal canine lung tissue to microwave coagulation is shown in Fig. 3. At 5 mm from the electrode (Fig. 3A), the temperature rose rapidly over 80°C (15 s for 60 W: 83.1 ± 13.0°C; 30 s for 40 W: 83.9 ± 3.4°C), and thereafter the temperature reached a plateau around 90-100°C at both 40 and 60 W. There was no significant difference between the two groups for each time point. At 20 W, the temperature rose gradually to only 65°C and reached a plateau. At 10 mm from the electrode (Fig. 3B), the temperature rose gradually to 70°C (45 s for 60 W: 70.6 ± 11.6°C; 90 s for 40 W: 70.9 ± 13.0°C), and thereafter the temperature reached a plateau around 80°C at 40 and 60 W. There was no significant difference between the two groups for each time point. At 20 W, the temperature rose to only 50°C after 90 s and reached a plateau. It appeared that 20 W was not enough for coagulation. The same thermal re-

FIG. 2. Microwave coagulation was performed using a microwave generator that emitted 2450 MHz microwaves of 12 cm wavelength at a power output of 20, 40, and 60 W.